Variable Background Active Contour Model for Computer-Aided Delineation of Nodules in Thyroid Ultrasound Images

Dimitris E. Maroulis, *Member, IEEE*, Michalis A. Savelonas, Dimitris K. Iakovidis, *Member, IEEE*, Stavros A. Karkanis, *Member, IEEE*, and Nikos Dimitropoulos

***Abstract*—This paper presents a computer-aided approach for nodule delineation in thyroid ultrasound (US) images. The developed algorithm is based on a novel active contour model, named variable background active contour (VBAC), and incorporates the advantages of the level set region-based active contour without edges (ACWE) model, offering noise robustness and the ability to delineate multiple nodules. Unlike the classic active contour models that are sensitive in the presence of intensity inhomogeneities, the proposed VBAC model considers information of variable background regions. VBAC has been evaluated on synthetic images, as well as on real thyroid US images. From the quantification of the results, two major impacts have been derived: 1) higher average accuracy in the delineation of hypoechoic thyroid nodules, which exceeds 91%; and 2) faster convergence when compared with the ACWE model.**

***Index Terms*—Active contour models, computer-aided diagnosis, level sets, thyroid nodules, ultrasound (US).**

I. Introduction

THYROID nodules are solid or cystic lumps formed in the thyroid gland, and can either be benign or malignant. Their prevalence increases with age and extends to more than 50% of the world's population [1]. Noninvasive medical imaging techniques such as magnetic resonance tomography (MRI), computerized tomography (CT), and ultrasonography, supervised by expert radiologists contribute to the early detection, assessment, and follow up of the nodules [2]. However, the subjectivity involved in the interpretation of the medical images made by these techniques can be regarded as their major drawback. A system that would be able to interpret these images based on explicit features could contribute to the objectification of medical diagnosis, as it could provide the experts with a second opinion, and could lead to a consequent reduction in misdiagnosis rates.

Manuscript received June 13, 2005; revised October 13, 2006. This work was supported in part by the Greek General Secretariat of Research and Technology and in part by the European Social Fund through the PENED 2003 program under Grant 03-ED-662.

D. E. Maroulis, M. A. Savelonas and D. K. Iakovidis are with the Realtime Systems and Image Analysis Group, Department of Informatics and Telecommunications, University of Athens, Athens 15784, Greece (e-mail: rtsimage@di.uoa.gr; msavel@di.uoa.gr; dimitris.iakovidis@ieee.org).

S. A. Karkanis is with the Department of Informatics and Computer Technology, Technological Educational Institute of Lamia, Lamia 35100, Greece (e-mail: sk@teilam.gr).

N. Dimitropoulos is with the Euromedica S.A. Medical Center, Department of Radiology, Athens 11527, Greece (e-mail: n.dimitropoulos@euromedica.gr).

Digital Object Identifier 10.1109/TITB.2006.890018

Ultrasonography is recognized as a cost-effective imaging technique, which does not involve ionizing radiations. It combines short acquisition times and sensitivity in ascertaining the size and the number of the thyroid nodules while providing additional information on their structure and characteristics. Nevertheless, the quality of the ultrasound (US) images produced is highly affected by noise that could hardly be modeled [3]. Consequently, a thyroid-nodule-detection methodology should take into account their inherent noise characteristics.

Among the various proposed approaches, active contour models have been gaining an increasing interest in US image analysis as they are self-adapting, and lead to continuous, closed, or open curves, without requiring edge-linking operations. Moreover, they can be relatively insensitive to noise by involving integral operators, which provide an inherent noise filtering mechanism [4].

Active contour models are classified into two main classes, according to their representation and implementation: the parametric active contours and the level set active contours. The latter are capable of detecting multiple objects in an image, whereas the former are not so flexible to allow topological changes of the contour during its evolution as required in such cases.

Active contour models have been employed in various medical US image analysis applications either in parametric or in level set form. Parametric active contour applications include the detection/delineation of hepatic tumors [4], the delineation of lumen and media-adventitia border in sequential intravascular ultrasound (IVUS) frames [5], and the evaluation of margins for malignant breast tumor excision through mammotome, which is a vacuum-assisted breast biopsy system that uses a computer-guided probe [6]. Level set active contour applications include the automatic quantification of the ventricular function [7] and the segmentation of prostate [8] and cardiac US images [9]. To the best of our knowledge, no computer-aided approach to thyroid nodule delineation in US images has been proposed.

In this paper, we propose a novel level-set active contour model for the delineation of nodules in thyroid US images, which is based on the active contour without edges (ACWE) model [10]. The proposed model is called variable background active contour (VBAC), and introduces variable background regions to reduce the effects of intensity inhomogeneity, which is attributed to noise, tissue texture, and calcifications. Thus, VBAC achieves more accurate delineation of the thyroid nodules as well as faster convergence than ACWE.

The remainder of this paper is organized as follows. In Section II, background information on active contour models and the formulation of the ACWE model is provided. The proposed VBAC model is presented in Section III. The results of the application of VBAC on real thyroid US images are apposed in Section IV. In Section V, the results and the impact of the proposed model in thyroid nodule diagnosis are discussed. This study is summarized in Section VI.

II. Active Contour Models

A. Background

The core idea of the active contour approach is based on the deformation of initial contours toward the boundaries of the image regions to be segmented. The deformation is realized by the minimization of an energy functional, which has been designed so that its local minimum is reached at the target boundaries. The energy functional in its basic form comprises of two components; the first controls the smoothness of the contour, and the second is image dependent and forces the contour towards the boundary. The classic active contour approach is boundary-based utilizing local filtering techniques such as edge detection operators. In the case of noisy images such as US images, many edges may appear due to noise, and should consequently be smoothed by the application of a strong isotropic Gaussian filter. Such filtering introduces the risk of smoothing the target boundaries, and therefore, contour leakage effects may appear resulting in the diminution of the delineation accuracy [10]. Moreover, the parametric formulation of the classic active contour approach does not allow for changes in the topology of the evolving contour such as splitting or merging.

Efforts have been made to solve the aforementioned problems. Caselles *et al*. [11] introduced the geodesic active contour (GAC) model, which embodies the level set formulation originally proposed in [12], thus, providing topological adaptability. However, the GAC model uses gradients to guide contour evolution, and thus, it is unsuitable for noisy images as they contain noise-generated high gradients that may be falsely perceived as boundaries [10].

Chan and Vese [10] proposed the ACWE model, which is level set and region-based following the Mumford–Shah segmentation approach [13]. The ACWE model does not require input image smoothing, even if it contains noise. Therefore, the target boundaries are preserved, and could be accurately detected. The ACWE model allows the detection of objects whose boundaries are either smooth or not necessarily defined by gradient. In such cases, the boundary-based active contour models commonly fail and result in boundary leakage.

B. ACWE Model

The ACWE model as described in [10] has the form of a minimization problem: Let Ω be a bounded open subset of R^2 and $\partial\Omega$ its boundary. We seek for the infimum of the energy functional $F(c^+, c^-, C)$, represented as

$$\begin{aligned} F(c^+, c^-, C) = {} & \mu \text{Length}(C) \\ & + \lambda^+ \int_{\text{inside}(C)} |u_0(x,y) - c^+|^2 dxdy \\ & + \lambda^- \int_{\text{outside}(C)} |u_0(x,y) - c^-|^2 dxdy \end{aligned} \tag{1}$$

where $u_0 : \Omega \to R$ is the input image, $C(s) : [0,1] \to R^2$ is a piecewise parameterized curve, c^+ and c^- are the average value of u_0 inside and outside the curve, and parameters $\mu > 0$ and $\lambda^+, \lambda^- > 0$ are weights for the regularizing term and the fitting terms, respectively. This problem is a special case of the minimal partition problem for which the existence of minimizers has been proved in [14]. As in the minimum energy problem, the minimizer corresponds to the "equilibrium" of the regularizing and fitting terms that force the contour to stop.

In the level set method [12], $C \subset \Omega$ is represented by the zero level set of a Lipschitz function $\phi : \Omega \to R$, such that

$$\begin{aligned} C &= \{(x,y) \in \Omega : \phi(x,y) = 0\} \\ \text{inside}(C) &= \{(x,y) \in \Omega : \phi(x,y) > 0\} \\ \text{outside}(C) &= \{(x,y) \in \Omega : \phi(x,y) < 0\}. \end{aligned} \tag{2}$$

Using the 1-D Dirac measure δ and the Heaviside function H, which are defined, respectively, by

$$\delta(z) = \frac{d}{dz} H(z) \quad H(z) = \begin{cases} 1, & \text{if } z \geq 0 \\ 0, & \text{if } z < 0 \end{cases} \tag{3}$$

where $z \in R$, the average foreground and background intensities c^+ and c^- can be determined by

$$c^+(\phi) = \frac{\int_\Omega u_0(x,y) H(\phi(x,y)) dxdy}{\int_\Omega H(\phi(x,y)) dxdy} \tag{4}$$

$$c^-(\phi) = \frac{\int_\Omega u_0(x,y)(1 - H(\phi(x,y))) dxdy}{\int_\Omega (1 - H(\phi(x,y))) dxdy}. \tag{5}$$

By keeping c^+ and c^- fixed, and minimizing F with respect to ϕ, the associated Euler–Langrange equation for ϕ is deduced. For this purpose, slightly regularized versions of H and δ are considered. The regularized Heaviside function H_ε is a continuously differentiable function for all degrees of differentiation, and it is derived as

$$H_\varepsilon(z) = \frac{1}{2}\left(1 + \frac{2}{\pi} \arctan\left(\frac{z}{\varepsilon}\right)\right) \tag{6}$$

where as the corresponding regularized delta function δ_ε is derived from

$$\delta_\varepsilon = dH_\varepsilon / dz.$$

As $\varepsilon \to 0$, both approximations converge to H and δ. These approximations allow the algorithm to compute a global minimizer, as described in [10].

Parameterizing the descent direction by an artificial time $t \geq 0, \phi(t,x,y)$ [with $\phi(0,x,y) = \phi_0(x,y)$ defining the initial

contour] is determined by

$$\frac{\partial \phi}{\partial t} = \delta_(\phi)\left[\mu \mathrm{div}\left(\frac{\nabla \phi}{|\nabla \phi|}\right) - \lambda^+(u_0 - c^+)^2 + \lambda^-(u_0 - c^-)^2\right] = 0 \tag{7}$$

where $t \in (0, \infty), (x, y) \in \Omega$.

In a practical implementation, a quantitative criterion should force the algorithm to stop when the changes of ϕ fall below a threshold for a fixed number of iterations. When this criterion is satisfied it is assumed that the minimizer is found, and the corresponding equilibrium has been reached.

A limitation of the ACWE model is that it assumes approximately piecewise constant intensities for object and background regions. This assumption is violated in thyroid US images where intensity inhomogeneities are present in the background image region with a consequent negative impact on the delineation of hypoechoic nodules.

III. VBAC Model

Aiming to surpass the limitation of the ACWE model resulting from its assumption of approximately piecewise constant image intensities, and enhance the delineation accuracy of hypoechoic nodules in the presence of intensity inhomogeneities, we propose the VBAC model. This new model utilizes a variable background from which inhomogeneities are excluded.

The remaining background regions are expected to be approximately constant, and thus, the assumption of constant background intensities used in the ACWE model is better approximated. The intensity inhomogeneity affects c^-, which is defined in (5) as the average background intensity. The VBAC model incorporates a new c^-, which is calculated as the average of the remaining background when inhomogeneity regions are excluded.

We introduce the difference $\Delta(x, y)$ as

$$\Delta(x, y) = H(\phi(x, y) + a) - H(\phi(x, y)) \tag{8}$$

where α is a positive constant. Its value is determined so that $[-a, 0]$ defines the acceptable range of $\phi(x, y)$ for a point (x, y) to be included in the variable background. Equations (6) and (8) imply that the points (x, y) for which $\phi(x, y) \notin [-a, 0]$ result in $\Delta(x, y) \approx 0$. These points correspond to intensity inhomogeneities within the region of interest, cause abrupt changes of ϕ, and result in $H(\phi(x, y) + a) = H(\phi(x, y))$. Moreover, we assume that the initial contour as traced by ϕ_0 corresponds to a region of interest within the thyroid gland, and we employ $H(\phi_o)$ to restrict the calculation of the average foreground and background intensities c^+ and c^- over this region. Equations (4) and (5) are reformulated as

$$c^+(\phi) = \frac{\int_\Omega u_0(x, y) H(\phi(x, y)) H(\phi_0(x, y)) dxdy}{\int_\Omega H(\phi(x, y)) H(\phi_0(x, y)) dxdy} \tag{9}$$

$$c^-(\phi) = \frac{\int_\Omega u_0(x, y)(1 - H(\phi(x, y))) H(\phi_0(x, y)) \Delta(x, y) dxdy}{\int_\Omega (1 - H(\phi(x, y))) H(\phi_0(x, y)) \Delta(x, y) dxdy}. \tag{10}$$

Equation (10) imposes that a point $(x, y) \in \Omega$ is not included in the calculation of c^- if $\Delta(x, y) = 0$. The VBAC model is finally described by (7)–(10).

The steps of the VBAC algorithm are summarized as follows.

Step 1) Initialize $\phi = \phi_0$.
Step 2) Calculate Δ by (8).
Step 3) Calculate $c^+(\phi)$ and $c^-(\phi)$ by (9) and (10).
Step 4) Solve (7) to obtain a new ϕ.
Step 5) If a stationary solution ϕ of (7) is obtained then stop.
Step 6) Repeat Steps 2)–5).

As the algorithm proceeds, the term c^- varies, resulting in a variable background. The contour evolves until it finds the best separation between the foreground and the background remaining by excluding the points (x, y) for which $\phi(x, y) \notin [-a, 0]$. An example run of the algorithm is illustrated in Fig. 1. The initial contour, defined by the user to fall within the thyroid gland, is indicated with a dashed line over the original thyroid US image in Fig. 1(a). It should be noted that, in practice, a global minimizer of the energy functional (1) can be obtained independently of the position of the initial contour. Fig. 1(b) illustrates the background considered in two subsequent iterations of the VBAC algorithm. The corresponding contours and surfaces $\phi(x, y)$ are illustrated in Fig. 1(c) and (d), respectively. The sparsity of the background reveals the selectivity of VBAC. It is clear that pixels belonging to calcifications and other tissue inhomogeneities have been excluded from the background.

IV. Results

We performed two sets of experiments. In the first set, we applied the VBAC and ACWE models on synthetic US images whereas in the second set, we applied them on a set of real thyroid US images.

For the purposes of our study we adopted the image intensity as the supervising feature for the contour evolution to enable the delineation of lower intensity blobs such as hypoechoic thyroid nodules. Low echogenicity characterizes the majority of thyroid nodules, and especially, those that are suspects of malignancy [15]. The active contour algorithms were implemented in Microsoft Visual C++, and executed on a 3.2-GHz Intel Pentium IV workstation. The model constants used in the experiments were generally chosen as: $\lambda^+ = 5, \lambda^- = 5, \mu = 650$, and $a = 10^{-13}$ [10]. The selection of α is application dependent. In the case of our experiments, it has been observed that the segmentation results were almost unaffected by varying a within the same order of magnitude. We considered the overlap value OV as a measure of similarity between two delineated regions A and G [16]

$$\mathrm{OV} = \frac{A \cap G}{A \cup G}. \tag{11}$$

The region G corresponds to the "ground truth" delineation and A corresponds to the manual or to the active contour delineation. In the case of $\mathrm{OV} = 1$, the two delineated regions match perfectly.

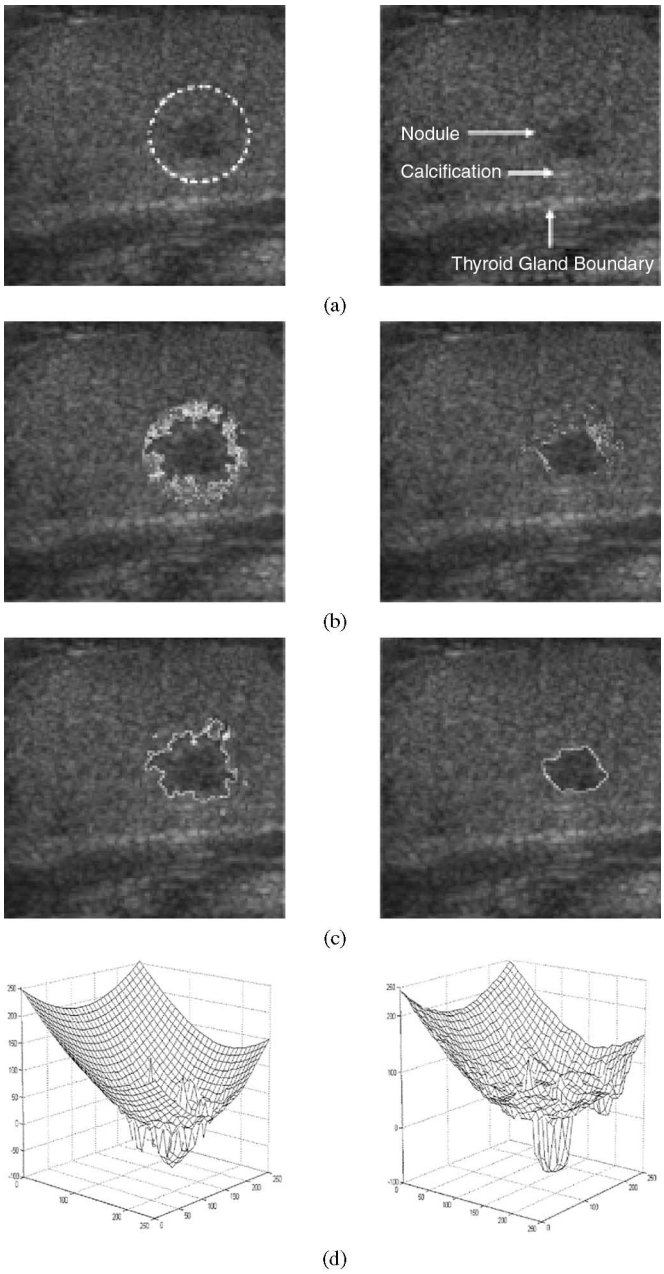

Fig. 1. Example run of the VBAC algorithm on a thyroid US image. (a) Original image (the dashed line indicates the initial contour). (b) Background regions marked with pixels of constant intensity around the nodule. (c) Corresponding contours. (d) Surfaces $\phi'(x, y) = -\phi(x, y)$ produced in two subsequent iterations.

A. Experiments on Synthetic Images

Preliminary experiments were performed in order to illustrate the advantages of VBAC over ACWE in presence of inhomogeneity, using two example synthetic images.

A B-mode image of a cyst phantom was simulated using the US simulation program field II [17]. The generation of the scatterers in the phantom involves the specification of their random position within a 60 mm $\times$ 40 mm $\times$ 15 mm cube, and the ascription of a Gaussian-distributed amplitude to each scatterer. If the scatterer resides within the cyst region, the amplitude is set to zero. A linear scan of the phantom was done with a 192-element transducer, using 64 active elements with a Hanning apodization in transmit and receive. A 256 $\times$ 256-pixel subimage of the resulting simulated image for 100 000 scatterers containing the cyst is illustrated in Fig. 2(b). The SNR of the simulated image is 3.5.

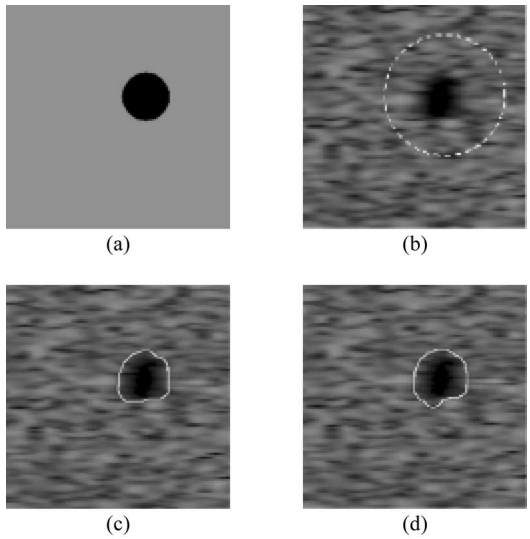

Fig. 2. Synthetic images. (a) Subimage of the echogenicity map. (b) Synthetic US image (the dashed line indicates the initial contour). (c) VBAC delineation. (d) ACWE delineation.

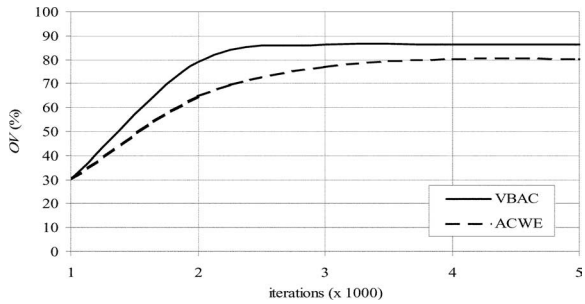

Fig. 3. Overlap values per iteration for the delineation of the cyst in Fig. 2(b).

First, the two active contour models were applied for the delineation of a dark blob in a 256 $\times$ 256-pixel image, which corresponds to the echogenicity map used for the generation of the synthetic image [Fig. 2(a)]. Both models achieved perfect delineation of the blob $(\mathrm{OV} = 100\%)$. This is reasonable because in the presence of homogeneous background the assumption of ACWE for piecewise constant intensity holds true. Therefore, ACWE is expected to converge to the target boundaries. Moreover, VBAC coincides with ACWE for homogeneous images regardless of the choice of a, provided that $-a < \phi_{\min}(\mathrm{outside}(C)) < 0$. In this case, there will not be any a such that (8) results in $\Delta(x, y) \approx 0$, and consequently, VBAC will also converge to the target boundaries.

Second, the models were applied for the delineation of the cyst region in Fig. 2(b). Fig. 2(c) showed that VBAC converged to an overlap value of 86.3% whereas the ACWE model converged to 80.3%, as shown in Fig. 2(d). The overlap values OV obtained per iteration are illustrated in Fig. 3.

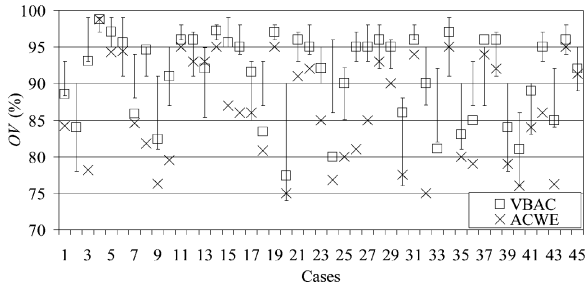

Fig. 4. Delineation results using VBAC and ACWE models. Vertical bars indicate the maximum and the minimum of the overlap values corresponding to the regions delineated by the expert radiologists. In cases 2 and 34, ACWE resulted in overlap values of 42.0% and 67.2%, respectively.

TABLE I
ANOVA RESULTS

Pair	Delineation 1	Delineation 2	p-value	F-ratio	95% Conf. Interval
1	ACWE	VBAC	4.4×10^{-4}	13.3	[-9.7, -2.9]
2	ACWE	Expert 1	4.6×10^{-9}	42.3	[-13.9, -6.5]
3	ACWE	Expert 2	3.7×10^{-2}	4.5	[-7.4, -0.4]
4	ACWE	Expert 3	5.8×10^{-5}	17.9	[-10.6, -3.2]
5	VBAC	Expert 1	2.0×10^{-4}	14.8	[-7.6, -0.2]
6	VBAC	Expert 2	4.1×10^{-2}	4.3	[-1.1, 6.3]
7	VBAC	Expert 3	5.6×10^{-1}	0.3	[-4.2, 3.0]
8	Expert 1	Expert 2	1.3×10^{-8}	39.3	[2.8, 10.2]
9	Expert 1	Expert 3	5.6×10^{-3}	8.1	[-0.4, 7.0]
10	Expert 2	Expert 3	3.0×10^{-4}	14.1	[-7.0, 0.4]

B. Experiments on Thyroid US Images

Thyroid US examinations were performed on 68 patients using a digital US imaging system HDI 3000 ATL with a 5–12-MHz linear transducer in the radiology department of Euromedica diagnostic center in Greece. A total of 71 longitudinal *in vivo* digital images of different thyroid nodule cases, some of which include multiple nodules, were acquired at a resolution of 256×256 pixels with a 256 grey-level depth. The dataset used in the experiment comprised of 45 hypoechoic nodule cases.

Three expert radiologists manually delineated the nodules on the thyroid US images to enable comparisons with the active contour models. For each image, ground truth delineation was obtained by following the rule that a pixel belongs to the nodule when it is included in at least two out of the three delineations drawn by the experts [18].

The delineation accuracies obtained by the two active contour models are illustrated in Fig. 4. In most cases, VBAC converges to higher overlap values than ACWE. The mean overlap values obtained with VBAC and ACWE are 91.1% and 84.8%, respectively. The mean difference of the overlap values obtained by the two models is 6.3 ± 3.4 in favor of VBAC. The statistical significance of this result was validated by one-way ANOVA [19]. The resulting F-ratio equals 13.3 with a p-value of 4.4×10^{-4}, which ensures that the mean difference is significant in a 0.0005 level (Table I, row 1). The corresponding 95% confidence interval is $[-9.7, -2.9]$.

One-way ANOVA was also applied for testing the statistical significance of the pairwise differences between the overlap values obtained by VBAC, ACWE, and each of the three experts. The results are summarized in Table I.

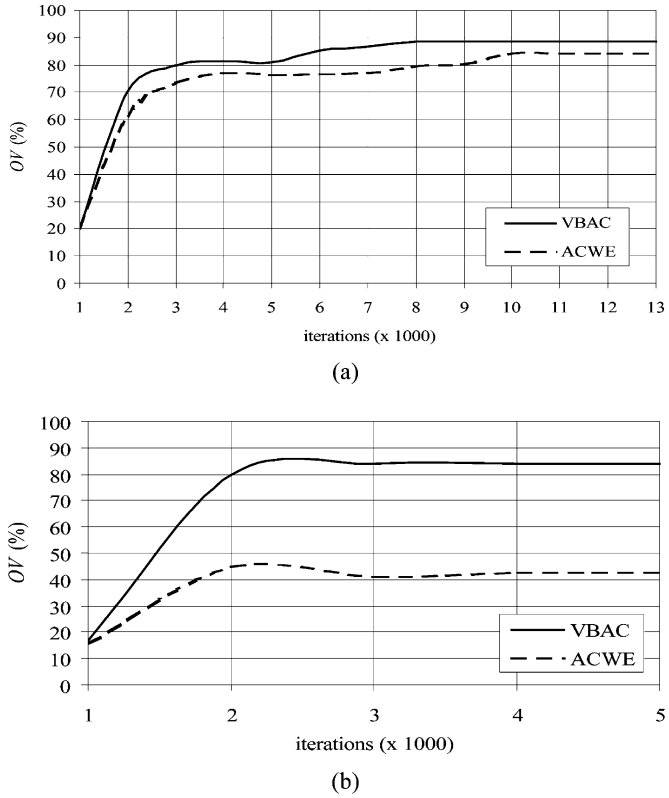

Fig. 5. Overlap values per iteration for two indicative thyroid US images. (a) Case 1. (b) Case 2.

Rows 2–4 of Table I show that the ACWE model is outperformed by all experts with $p \leq 3.7 \times 10^{-2}$. Rows 5–7 show that VBAC performs significantly better than expert 1 with $p = 2.0 \times 10^{-4}$ whereas it does not perform significantly worse than any other expert. Rows 8–10 show that the differences between the experts' delineations could be significant. Moreover, the interobserver variability as quantified by the coefficient of variation [20] ranges between 1.0% to 9.8%.

Both models achieved a maximum overlap value of 98.8% in case 4, which displays a clearly distinguishable nodule (Fig. 4). The minimum overlap value obtained with the VBAC model was 77.4% in case 20, whereas the ACWE model resulted in the lowest minimum overlap value of 42.0% in case 2.

Moreover, the vertical bars in Fig. 4 indicate the maximum and the minimum of the overlap values that correspond to the regions delineated by the expert radiologists to enable comparisons with the two active contour models. It can be observed that in 37 cases, VBAC results in overlap values that fall within the ranges obtained by the delineations drawn by the experts. The ACWE model converged within those ranges in only 15 cases.

The mean boundary difference between the A and G contours at convergence reached 3 pixels in the case of VBAC and 13 pixels in the case of ACWE. The clinical significance of the difference between the boundaries delineated by the two active contour models, when observed on a real thyroid US image, is mostly correlated with the shape information rather than the volumetric nodule characteristics. The shape of a thyroid nodule and the irregularity of its margins are malignancy risk factors

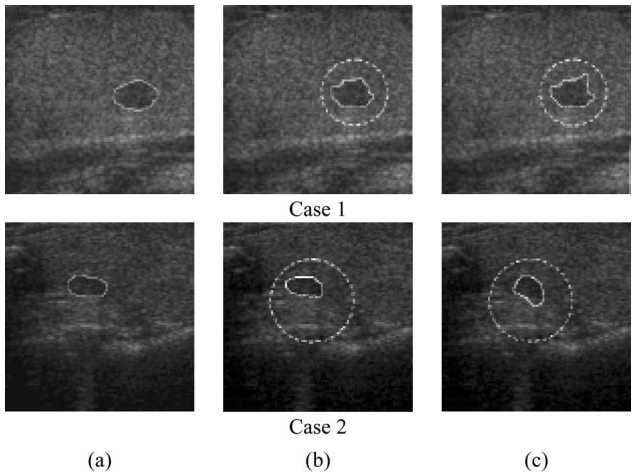

Fig. 6. Two thyroid US images with delineated nodules corresponding to the cases of Fig. 5. (a) Ground truth. (b) VBAC. (c) ACWE delineations. Initial contours are indicated with dashed lines.

that are always considered by the clinicians before proceeding to fine needle aspiration biopsy [15], [21].

Furthermore, the VBAC model converged in 9.6% less iterations on average than the ACWE model, which in turn results in approximately 8.2% speedup in terms of absolute execution time. The VBAC model requires 18.4 ms for a single iteration of the algorithm whereas ACWE requires 18.0 ms. The average segmentation times are 1 min and 33 s for VBAC, and 1 min and 41 s for ACWE. The overlap values obtained per iteration for two indicative cases are illustrated in Fig. 5. As in the first set of experiments, the diagrams show that VBAC converges in less iterations than ACWE. The corresponding delineations obtained at convergence as well as the user-defined initial contours are illustrated in Fig. 6. It is worth noting that identical contours were defined for the initialization of VBAC and ACWE so as to allow for direct comparisons of the results.

A particularly low overlap value is obtained with ACWE in case 2. This could be attributed to the large intensity inhomogeneity within the region of interest, as it is quantified by means of relative standard deviation (RSD), i.e., the standard deviation to mean ratio of image intensities. As a result, the assumption of ACWE for piecewise constant intensity is weaker.

V. Conclusion

We presented a novel active contour model, referred to as VBAC, which was applied for computer-aided delineation of nodules in thyroid US images. The new model incorporates the advantages of the level set and region-based ACWE model, which include noise robustness and multiple nodule delineation capabilities. Moreover, it copes with intensity inhomogeneity, which is dominant in thyroid US images, by considering background regions that vary throughout the iterations of the algorithm.

The proposed model was evaluated and compared with the ACWE model on synthetic and real thyroid US images. The results of the experimental study presented in this paper lead to the conclusions.

1) The experiments performed on synthetic images showed that the performance of VBAC is comparable to that of ACWE in homogeneous images. However, when inhomogeneity is introduced, VBAC outperforms ACWE.
2) In particular, the application of VBAC on thyroid US images leads to more accurate delineations of hypoechoic nodules than ACWE, in less iterations.
3) The manual delineations of the thyroid nodules indicate that the experts' subjectivity may lead to noticeable inter-observer variability. The estimated delineation accuracy of the proposed model is comparable to that of expert radiologists, which suggests that its application in clinical practice is feasible.
4) The proposed model contributes to the objectification of the diagnostic process by the utilization of explicit image features. Moreover, it can provide the diagnosticians with a second opinion on the delineation of thyroid nodules, and it could be proved a valuable tool in follow-up diagnosis where the validity of conclusions drawn by the comparison of subsequent delineations depends on the delineation accuracy.

The observations and conclusions made in this paper are being reinforced as more patients with hypoechoic thyroid nodules are added into our database. Efforts on the optimization of the VBAC algorithm are under way. Future perspectives of this work include the following:

1) embedment of additional features encoding texture [19], [22] to supervise contour evolution, which could enable the delineation of nonhypoechoic thyroid nodules;
2) derivation of additional information from video frame sequences for the identification of thyroid nodules;
3) extensions for color Doppler US images;
4) integration of heterogeneous information for the development of a medical decision support system for the identification of thyroid nodules.

References

[1] New York Thyroid Center. Available: http://cpmcnet.columbia.edu/dept/thyroid/.
[2] E. J. Mackenzie and R. H. Mortimer, "Thyroid nodules and thyroid cancer," *Med. J. Aus.*, vol. 180, pp. 242–247, 2004.
[3] S. V. B. Jardim and M. A. T. Figueiredo, "Automatic contour estimation in fetal ultrasound images," in *Proc. ICIP*, vol. 2, Barcelona, Spain, Sep. 2003, pp. 065–1073.
[4] C. M. Chen, H. H. S. Lu, and A. T. Hsiao, "A dual-snake model of high penetrability for ultrasound image boundary extraction," *Ultrasound Med. Biol.*, vol. 27, no. 12, pp. 1651–1665, 2001.
[5] M. E. Plissiti, D. I. Fotiadis, L. K. Michalis, and G. E. Bozios, "An automated method for lumen and media-adventitia border detection in a sequence of IVUS frames," *IEEE Trans. Inf. Technol. Biomed.*, vol. 8, no. 2, pp. 131–141, Jun. 2004.
[6] R. F. Chang, W. J. Wu, C. C. Tseng, D. R. Chen, and W. K. Moon, "3-D snake for US in margin evaluation for malignant breast tumor excision using mammotome," *IEEE Trans. Inf. Technol. Biomed.*, vol. 7, no. 3, pp. 197–201, Sep. 2003.
[7] E. Angelini, J. Holmes, and A. Laine, "Segmentation of RT3D ultrasound with implicit deformable models without gradients," in *Proc. ISPA 2003*, vol. 2, Rome, Italy, Sep. 2003, pp. 711–716.
[8] D. Honigmann, J. Ruisz, and H. Pottmann, "Fast model based segmentation of ultrasound data using an active image," in *Proc. IEEE Int. Symp. Biomed. Imag.*, Washington, DC, 2002, pp. 225–228.

[9] N. Lin, W. Yu, and J. S. Duncan, "Combinative multi-scale level set framework for echocardiographic Image segmentation," *Med. Image Anal.*, vol. 7, pp. 529–537, 2003.
[10] T. F. Chan and L. A. Vese, "Active contours without edges," *IEEE Trans. Image Process.*, vol. 10, no. 2, pp. 266–277, Feb. 2001.
[11] V. Caselles, R. Kimmel, and G. Sapiro, "Geodesic active contours," *Int. J. Comput. Vision*, vol. 22, pp. 61–79, 1997.
[12] S. Osher and J. Sethian, "Fronts propagating with curvature-dependent speed: Algorithms based on the Hamilton–Jacobi formulations," *J. Comput. Phys.*, vol. 79, pp. 12–49, 1988.
[13] D. Mumford and J. Shah, "Optimal approximation by piecewise smooth functions and associated variational problems," *Commun. Pure Appl. Math.*, vol. 42, pp. 577–685, 1989.
[14] J. M. Morrel and S. Solimini, "Segmentation of images by variational methods: A constructive approach," Rev. Math. Univ. Comput. Madrid, Spain, vol. 1, pp. 169–182, 1988.
[15] E. Papini *et al.*, "Risk of malignancy in nonpalpable thyroid nodules: Predictive value of ultrasound and color-Doppler features," *J. Clin. Endocrinol. Metab.*, vol. 87, no. 5, pp. 1941–1946, 2002.
[16] X. Hao, C. Bruce, C. Pislaru, and J. F. Greenleaf, "A novel region growing method for segmenting ultrasound images," *IEEE Int. Ultrason. Symp.,* San Juan, PR, vol. 2, pp. 1717–1720, Oct. 2000.
[17] J. A. Jensen, "Field: A program for simulating ultrasound images," *Med. Biol. Eng. Comput.*, vol. 34, no. 1, pp. 351–353, 1996.
[18] M. R. Kaus, S. K. Warfield, F. A. Jolesz, and R. Kikinis, "Segmentation of meningiomas and low grade gliomas in MRI," in *Proc. Int. Conf. Med. Image Comp. Comp.-Assist. Interv.*, Cambridge, U.K., 1999, pp. 1–10.
[19] S. Theodoridis and K. Koutroumbas, *Pattern Recognition*. New York: Academic, 1998.
[20] H. H. Woltjer, "The intra- and interobserver variability of impedance cardiography in patients at rest during exercise," *Physiol. Meas.*, vol. 17, pp. 171–178, 1996.
[21] E. Koike *et al.*, "Ultrasonographic characteristics of thyroid nodules: Prediction of malignancy," *Arch. Surg.*, vol. 136, pp. 334–337, 2001.
[22] B. Sandberg, T. Chan, and L. Vese, "A level-set and Gabor-based active contour algorithm for segmenting textured images," Math. Dept., UCLA, Tech. Rep. 39, Jul. 2002.

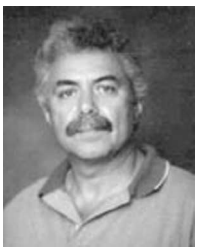

Dimitris E. Maroulis (M'02) received the B.Sc. degree in physics, M.Sc. degrees in radioelectricity and cybernetics, and Ph.D. degree in informatics from the University of Athens, Athens, Greece, in 1973, 1977, 1980, and 1990, respectively.

Currently, he is an Associate Professor in the Department of Informatics and Telecommunications, University of Athens. He is the coauthor of more than 90 articles in scientific journals and conference proceedings on data acquisition systems, real time systems, image analysis, and biomedical applications. His research interests include biomedical, data acquisition, real-time, image/signal processing systems, and bioinformatics.

Michalis A. Savelonas received the B.Sc. degree in physics and M.Sc. degree (with honors) in cybernetics, from the University of Athens, Athens, Greece in 1998 and 2001, respectively, and is currently working toward the Ph.D. degree in medical image analysis at the University of Athens.

Earlier, he was a Software Engineer for the development of real time systems.

Dimitris K. Iakovidis (M'05) received the B.Sc. degree in physics, M.Sc. degree (with honors) in cybernetics, and Ph.D. degree in medical informatics, from the University of Athens, Athens, Greece, in 1997, 2001, and 2004, respectively.

Currently, he is a Research Fellow in the Department of Informatics and Telecommunications, University of Athens. He is the coauthor of more than 30 papers on biomedical applications and image analysis and is a reviewer in many international journals. His research interests include biomedical systems, image analysis, pattern recognition, and bioinformatics.

Stavros A. Karkanis (M'89) received the B.Sc. degree in mathematics and Ph.D. degree in informatics and telecommunications from the University of Athens, Athens, Greece, in 1986 and 1995, respectively.

Currently, he is an Associate Professor in the Department of Informatics and Computer Technology, Technological Educational Institute of Lamia, Lamia, Greece. His research interests include texture recognition, wavelet transform for texture, pattern recognition for image processing applications, and statistical learning methodologies for classification.

Nikos Dimitropoulos received the M.D. degree from the University of Patras, Patras, Greece, in 1985, and the Ph.D. degree from the Medical School of the University of Athens, Athens, Greece, in 1994.

Currently, he is with Euromedica S.A. Medical Center, Department of Radiology, Athens, Greece. He is the coauthor of many journal papers in the field of radiology, in which he has more than 20 years of experience, especially in the diagnosis of thyroid diseases.